Tuijin Jishu/Journal of Propulsion Technology
ISSN: 1001-4055
Vol. 45 No. 3 (2024)

Battery Health Aware Energy Management Strategy for Hybrid Electric Vehicle using Artificial Neural Networks

Anılcan Özkan [1], Xianke Lin [2], Osman Taha Sen [3], Senem Kurşun [4]
[1, 3, 4] *Department of Mechanical Engineering, Istanbul Technical University, Istanbul, Turkey*
[1, 2] *Department of Automotive and Mechatronics Engineering, Ontario Tech University, Oshawa, Canada*

Abstract: Battery health aware energy management strategy (EMS) is designed for a power-split hybrid electric vehicle (HEV) by using Artificial Neural Networks (ANN). Three different speed profiles are selected to obtain a dataset. WLTP is used as the dynamic, transient speed profile, HWFET is used as the highway speed profile and NEDC is used as the third speed profile. Vehicle is operated in charge-sustaining mode in these drive cycles by using Equivalent Consumption Minimization Strategy (ECMS). Three different initial State-of-Charge (SOC) values are used in simulations. Each cycle is run for three different initial SOC values. Two ANN controllers are designed to control ICE torque and speed. Torque demand of the vehicle, SOC, and battery capacity fade are selected as the inputs of the ANN. The goal of this study is the investigation of battery degradation and fuel consumption by using ANN. Results for WLTP show that capacity fade can be reduced up to 14.85% and fuel consumption can be reduced 3.83% for the lowest initial SOC value. For intermediate initial SOC value, capacity fade is reduced by 13.80% and fuel consumption is reduced by 1.84%. For highest initial SOC value, capacity fade is reduced by 14.70 % with the 5.75% increase of fuel consumption. Results are consistent for the other two drive cycles. Battery degradation is also reduced in HWFET and NEDC.

Keywords: Artificial neural networks, battery degradation, ECMS, hybrid electric vehicle.

1. Introduction

Due to the limited reserves of fossil fuels and harmful emissions, countries all around the world are assessing the benefits of electrification in transportation [1]-[3]. Electric motors offer quiet operation and excellent acceleration performance but battery technology still needs improvements because of their cost and range limitations. Hybrid electric vehicles (HEVs) are another alternative for the electrification of transportation. HEVs can decouple internal combustion engines from driven wheels and operate them in an efficient region. HEVs can increase the fuel economy and due to smaller battery packs, compared to battery electric vehicles (BEVs), they are less expensive than BEVs. Energy management strategy (EMS) plays a key role for HEVs because of the operation of different powertrain components. HEV EMSs can be classified as optimization based methods, rule based methods and machine learning methods. Many different EMS algorithms are present in the literature. Until the last decade, most of the EMS research on HEVs was focused on the reduction of the fuel consumption. With the increasing number of BEVs and HEVs and the battery costs, researchers started to take battery degradation into account. Battery health conscious EMSs designed over the last years by using many different algorithms such as global and instantaneous optimization algorithms, rule based methods and machine learning methods. Dynamic Programming (DP) is the most common global optimization algorithm and Equivalent Consumption Minimization Strategy (ECMS) is an instantaneous optimization algorithm that can achieve close results to DP. Fuzzy Logic is investigated for HEVs as a rule based method and proved that based on human intuition and expertise, satisfactory results can be achieved. Artificial Neural Networks (ANN) also gained attention from researchers in the last years and are used for different HEV applications. Literature Review below provides a summary of ANN methods used for HEV applications.

ANN has the ability to decipher complex non-linear relationships and emerge as a preferred tool for health management of lithium-ion batteries [4]. Various ANN architectures have been employed to predict the state of batteries including Convolutional Neural Network (CNN), Recurrent Neural Network (RNN), Feedforward Neural Network (FNN) [4].

A new Radial Basis Function Neural Network (RBFNN) is built in [5] and SOC estimation accuracy was increased. In [6], ANN is used for aging prediction and SOC estimation of a $LiFePO_4$ battery. Input time-delayed neural network technique is used and accurate state of charge and state of health estimation were achieved simultaneously. In [7], RNN is used for battery degradation prediction and compared to existing methods, proposed method predicts more accurately.

Apart from health management of lithium-ion batteries, ANN has been used for other HEV applications such as component sizing of a series HEV in [8]. In [9], ANN is used to enhance the EMS of the HEV and satisfactory fuel economy results were achieved. In [10], another neural network-based EMS is designed for a plug-in HEV and reductions in the fuel consumptions were observed. As seen in the above examples, ANN can be used both for battery health management, SOC and degradation estimations of a hybrid electric vehicle and fuel consumption optimization, which are both important for HEVs and EMS design. This paper aims to investigate ANN as a battery health conscious EMS for a power-split HEV. For this end, a dataset is obtained for charge-sustaining operation of the vehicle by using ECMS and battery capacity fade input is used in ANN controllers. Matlab Neural Networks toolbox is used to design ANN controllers and dataset is divided into 70% training data, 15% testing data and 15% validation data. Two ANN controllers are designed to control ICE torque and speed with the inputs of torque request of the vehicle, SOC and capacity fade. Three different speed profiles are selected as one dynamic transient profile, one highway speed profile and one intermediate speed profile. Designed ANN controllers are tested in all speed profiles and results show that battery degradation is reduced in all cases. The rest of this paper is organized as follows; Section 2 explains the vehicle model, Section 3 explains implementation of ECMS, Section 4 explains ANN implementation, Section 5 compares the results of ECMS and ANN for all drive cycles and Section 6 includes conclusions.

2. Vehicle Model

A power-split HEV is modeled by using backward quasi-static approach [11] in Simulink. The traction force required is calculated by the equation;

$$F_t = F_r + F_{aero} + F_{acc} \quad (1)$$

where F_t is the traction force, F_r is the rolling resistance, F_{aero} is the aerodynamic resistance and F_{acc} is the acceleration resistance. Rolling resistance, aerodynamic resistance and acceleration resistance are calculated by the equations given below.

$$F_r = mgfr \quad (2)$$

$$F_{aero} = \frac{1}{2}\rho C_D A_f V^2 \quad (3)$$

$$F_{acc} = ma\delta \quad (4)$$

$$f_r = 0.01(1 + \frac{3.6}{160} V) \quad (5)$$

$$\delta = 1.04+0.0025 i_{FD}^2 \quad (6)$$

where m is the vehicle mass (kg), g is the gravitational acceleration (m/s^2), f_r is the rolling resistance coefficient, ρ is the air density (kg/m^3), C_D is the aerodynamic coefficient, A_f is the frontal area of the vehicle (m^2), V is the vehicle speed (m/s), a is the acceleration of vehicle (m/s^2), δ is the rotational inertia factor and i_{FD} is the final drive ratio. Rotational effect of planetary gear set is not taken into account for simplification, just the rotational effect of final drive is included in the vehicle model. After required traction force is calculated, wheel torque and torque request are calculated by the equations given below.

$$T_{wheel} = F_t\, r_w \quad (7)$$

$$T_{req} = \frac{T_{wheel}}{i_{FD}} \quad (8)$$

where T_{wheel} is the torque at the wheels in Nm, r_w is the wheel radius in meter and T_{req} is the torque request of the vehicle. Vehicle parameters used to calculate traction force and wheel torque are given below in Table 1 and power-split configuration used in this study is given below in Fig. 1.

Table 1: Vehicle parameters

Vehicle mass (m)	1361 kg
Air density (ρ)	1.23 kg/m^3
Aerodynamic coefficient (C_D)	0.26
Frontal Area (A_f)	2.33 m^2
Final drive ratio (i_{FD})	3.267
Wheel radius (r_w)	0.31075 meter

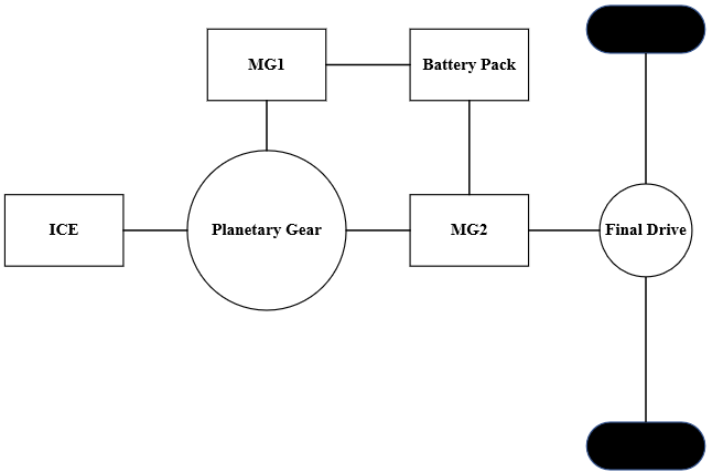

Fig. 1: Power-split configuration

Internal combustion engine (ICE) is connected to the carrier of the planetary gear, Motor/Generator 1 (MG1) is connected to sun gear and Motor/Generator 2 (MG2) is connected to driven wheels. ICE power is split in planetary gear to charge the battery pack through MG1 and provide traction torque through ring gear. Torque request of the vehicle, T_{req} is the combination of the torque provided by MG2 and ICE torque through ring gear. Torque and speed equations of the planetary gear set are given below.

$$T_{req} = T_r + T_{MG2} \quad (9)$$

$$T_r = \frac{T_{ICE}}{1+i_{PG}} \quad (10)$$

$$T_{MG1} = T_r\, i_{PG} = T_{ICE}\, \frac{i_{PG}}{1+i_{PG}} \quad (11)$$

where T_r is the torque at ring gear, output of the planetary gear in Nm, T_{MG2} is the torque of MG2, T_{ICE} is the torque of internal combustion engine, T_{MG1} is the torque of MG1 and i_{PG} is the planet gear ratio, which is number of teeth of sun gear (N_s) divided by number of teeth of ring gear (N_r). Angular velocities of the components are given in below equations.

$$\omega_{wheel} = \frac{V}{r_w} \quad (12)$$

$$\omega_{MG2} = \omega_r = \omega_{wheel}\, i_{FD} \quad (13)$$

where ω_{wheel} is the wheel angular velocity in rad/s, ω_{MG2} is the angular velocity of MG2 in rad/s and ω_r is the angular velocity of ring gear in rad/s. Angular velocities of MG2 and ring are equal and proportional to the angular velocity of the wheels. Speed equation of the planetary gear set is given below and powertrain specification are given in Table 2.

$$(1 + i_{PG})\omega_{ICE} = i_{PG}\, \omega_{MG1} + \omega_{MG2} \quad (14)$$

Table 2: Powertrain specifications

Maximum Torque of ICE	115 Nm@4200 rpm
Maximum Speed of ICE	5000 rpm
Maximum Torque of Electric Motor (MG2)	400 Nm
Maximum Speed of Electric Motor (MG2)	6000 rpm
Maximum Torque of Generator (MG1)	145 Nm
Maximum Speed of Generator (MG1)	10000 rpm
Number of teeth of sun gear N_s	30
Number of teeth of sun gear N_r	78
Planet gear ratio, i_{PG} $(\frac{N_s}{N_r})$	0.384

In this study, ICE torque and speed are determined by the vehicle controller. As seen in above equations, when the ICE torque and speed are determined by the control algorithm, torque of MG2, torque of MG1 and speed of MG1 can be determined from planet gear equations. By using these parameters, battery power, P_{Batt}, is calculated as follows;

$$P_{Batt} = \frac{T_{MG1}\omega_{MG1}}{\eta_{MG1}^{sign(T_{MG1}\omega_{MG1})}} + \frac{T_{MG2}\omega_{MG2}}{\eta_{MG2}^{sign(T_{MG2}\omega_{MG2})}} \quad (15)$$

Battery model and Capacity Fade model

Battery is modeled as a zeroth order equivalent circuit model. Battery cell power is calculated as follows for a zeroth order equivalent circuit model.

$$P_{batt} = V_{oc}I - R_{in}I^2 \quad (16)$$

where V_{oc} is the open circuit voltage, I is the battery current and R_{in} is the internal resistance. $LiFePO_4$battery cells are used in the model and cell parameters are given below in Table 3.

Table 3: Cell parameters

Nominal capacity (Ah)	2.5
Nominal Voltage (V)	3.3
Maximum discharge current (A)	50

Capacity fade model in [12] is used as the degradation model.

$$Q_{cyc} = (\alpha SOC + \beta).\exp\left(\frac{-E_a + \eta\, C_{rate}}{R_{gas}T_K}\right)Ah^z \quad (17)$$

where α and β are fitting coefficients, $E_a$is the activation energy, η is the compensation factor of C_{rate}, R_{gas} is the gas constant, T_K is the ambient temperature in (K), Ah is the Ah-throughput and z is the power law factor. Parameters of the capacity fade model are given below in Table 4.

Table 4: Aging model parameters

Fitting coefficient α	$\begin{cases} 2896.6, & SOC \leq 0.45 \\ 2694.5, & SOC > 0.45 \end{cases}$
Fitting coefficient β	$\begin{cases} 7411.2, & SOC \leq 0.45 \\ 6022.2, & SOC > 0.45 \end{cases}$
η	152.5
$E_a(\frac{\mathrm{J}}{\mathrm{mol}})$	31,500
$R_{gas}(J/(\mathrm{mol.K})$	8.314
z	0.57

3. Equivalent Consumption Minimization Strategy

To obtain a dataset for ANN, ECMS is used. ECMS was first introduced by Paganelli [13] and used extensively in the literature. It can achieve results close to global optimization algorithms such as DP. ICE torque and speed are controlled by using ECMS for the charge sustaining operation of the HEV. The ECMS is based on the notion that, in charge-sustaining hybrid electric vehicles, the difference between the initial and final state of charge of the battery is very small, negligible with respect to the total energy used. This means that all energy comes from fuel, and the battery can be seen as an auxiliary, reversible fuel tank [14].

ICE torque and speed are discretized as the control variables. Fuel rate of the engine $\dot{m}_f$ in kg/s is a function of ICE torque and speed.

$$\dot{m}_f = f(T_{ICE}, \omega_{ICE}) \tag{18}$$

Since ICE is not connected to the driven wheels in the power-split configuration, it can be operated at the most efficient region. Cost function, J, of ECMS can be written as follows:

$$\mathrm{J} = P_{ICE} + \lambda\, p(SOC) P_{batt} \tag{19}$$

$$P_{ICE} = \dot{m}_f\, Q_{lhv} \tag{20}$$

$$p(SOC) = 1 - \left(\frac{SOC(t) - SOC_{target}}{(SOC_{max} - SOC_{min})/2}\right)^3 \tag{21}$$

where P_{ICE} is the fuel power of ICE (kW), λ is the equivalence factor and $p(SOC)$ is the penalty function for state-of-charge, Q_{lhv} is the lower heating value of the fuel (MJ/kg). Initial value of equivalence factor is taken as 3.385 and a dicrete PI block is used for adaptation of equivalence factor. Implemented ECMS is subjected to following powertrain constraints;

$$\omega_{ICE,min} \leq \omega_{ICE} \leq \omega_{ICE,max} \tag{22}$$

$$T_{ICE,min} \leq T_{ICE} \leq T_{ICE,max} \tag{23}$$

$$\omega_{MG1,min} \leq \omega_{MG1} \leq \omega_{MG1,max} \tag{24}$$

$$T_{MG1,min} \leq T_{MG1} \leq T_{MG1,max} \tag{25}$$

$$\omega_{MG2,min} \leq \omega_{MG2} \leq \omega_{MG2,max} \tag{26}$$

$$T_{MG2,min} \leq T_{MG2} \leq T_{MG2,max} \tag{27}$$

$$SOC_{min} \leq SOC \leq SOC_{max} \tag{28}$$

$$I_{batt,min} \leq I_{batt} \leq I_{batt,max} \tag{29}$$

Simulink model of ECMS and equivalence factor are given below in Figs 2-3.

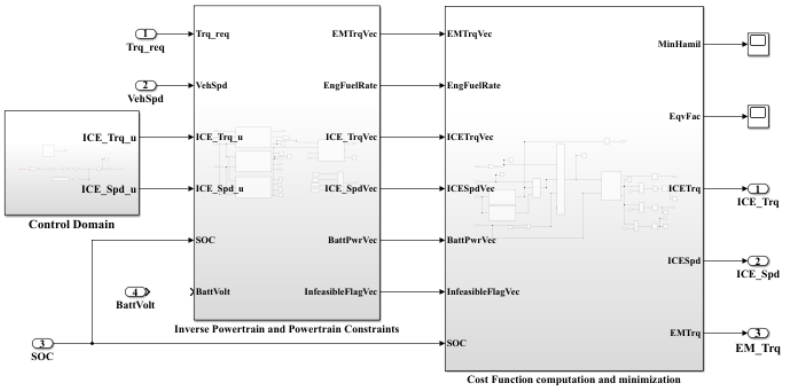

Fig. 2: ECMS Controller in Simulink

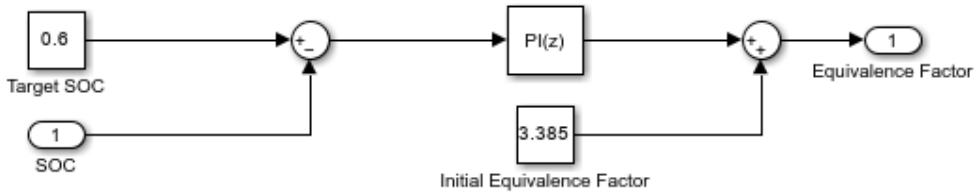

Fig. 3: Equivalence factor adaptation based on SOC

After ECMS is implemented in the vehicle model, three different speed profiles are selected. Worldwide Harmonised Light Vehicles Test Procedure (WLTP) is selected as the most dynamic, transient drive cycle which represents real driving conditions. The Highway Fuel Economy Test (HWFET) drive cycle is selected as the highway speed profile and New European Driving Cycle (NEDC) is selected as an intermediate speed profile. Vehicle is operated in charge sustaining mode for three different initial SOC values. SOC values are selected as 20% as the lowest SOC, 60% as the medium SOC and 80% as the highest SOC. For each drive cycle, three different simulations are conducted for different initial SOC values and in total, nine simulations are conducted to obtain a dataset. Drive cycles and results of ECMS are given below.

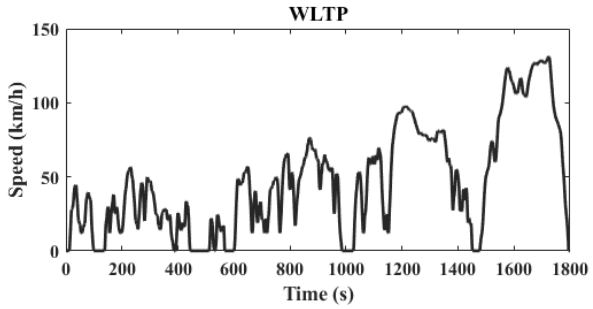

Fig. 4: WLTP Speed- Time graph

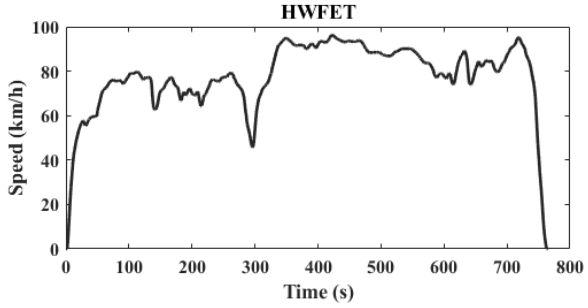

Fig. 5: HWFET Speed-Time graph

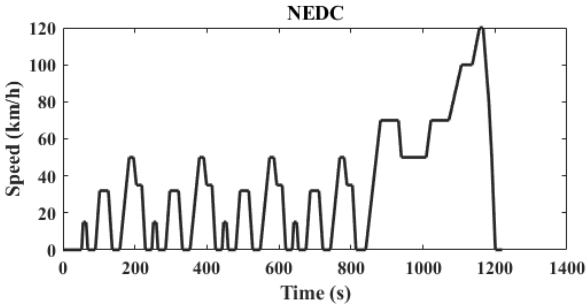

Fig. 6: NEDC Speed-Time graph

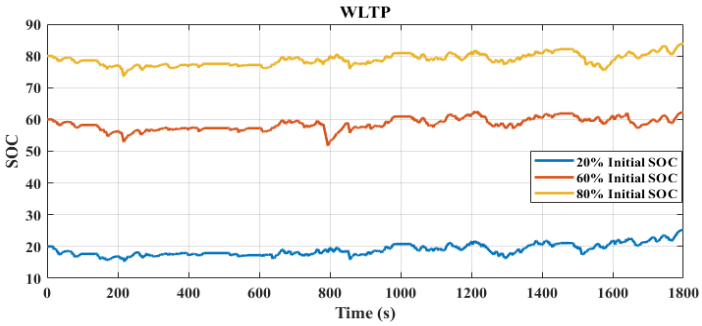

Fig. 7: WLTP SOC- Time graph

Fig. 7 shows SOC profiles in WLTP drive cycle for different initial SOC levels, as seen in Fig.7, vehicle is operated in charge-sustaining mode in all cases. The reason to choose low, medium and high SOC levels is that the SOC is one of the parameters in the aging model.

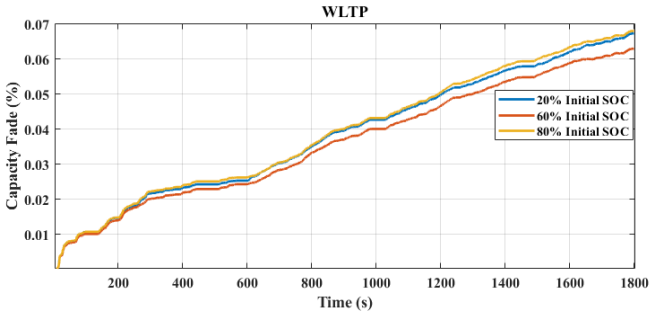

Fig. 8: WLTP Capacity Fade-Time graph

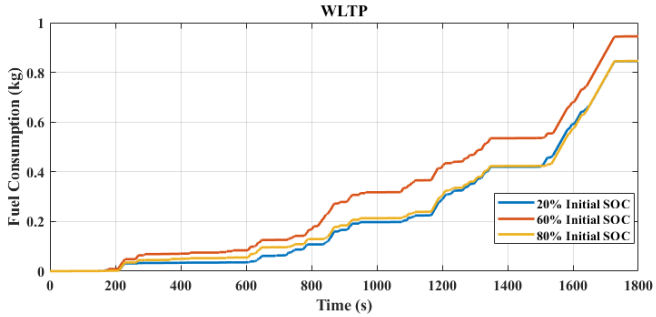

Fig. 9: WLTP Fuel Consumption-Time graph

Figs. 8-9 show capacity fade and fuel consumptions results for WLTP drive cycle. As seen in these results, there is a trade-off between battery usage and fuel consumption. Fig. 8 shows that minimum battery degradation occurs for 60% initial SOC level, which is the highest fuel consumption according to Fig. 9. For low and high SOC levels, battery degradation and fuel consumption are very close, as seen in Figs. 8-9.

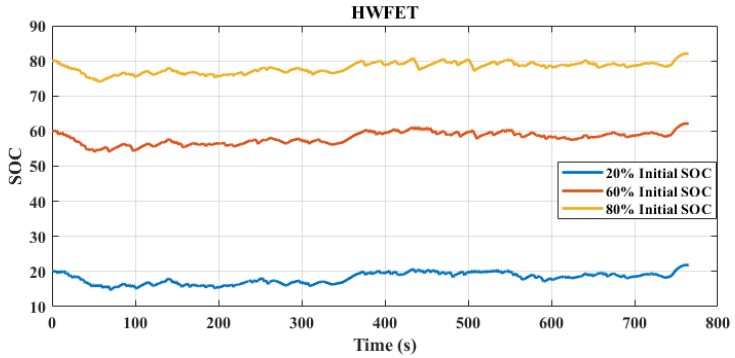

Fig. 10: HWFET SOC-Time graph

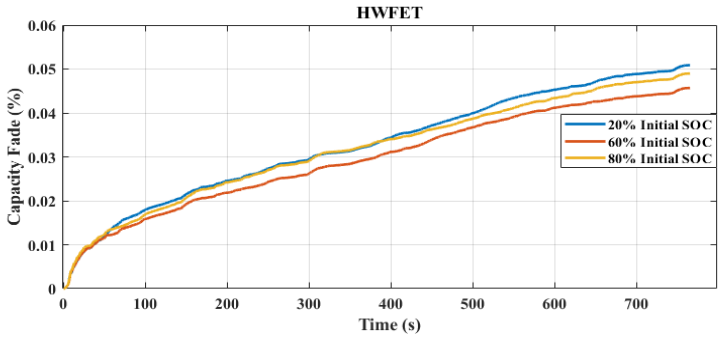

Fig. 11: HWFET Capacity Fade-Time graph

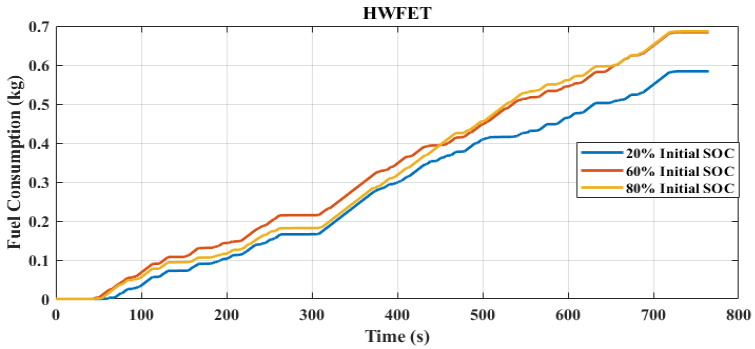

Fig. 12: HWFET Fuel Consumption-Time graph

Figs. 10-12 show ECMS results for HWFET drive cycle. The trade-off between battery degradation and fuel consumption can be seen in this drive cycle as well. Fig. 11 shows that capacity fade is highest for lowest SOC level, 20%. In this case, more battery power is used, therefore fuel consumption is reduced as seen in Fig. 12. Compared to intermediate and high SOC levels, fuel consumption is minimum for 20% SOC level.

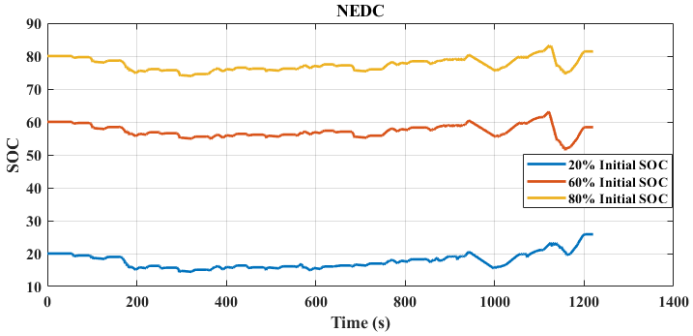

Fig. 13: NEDC SOC-Time graph

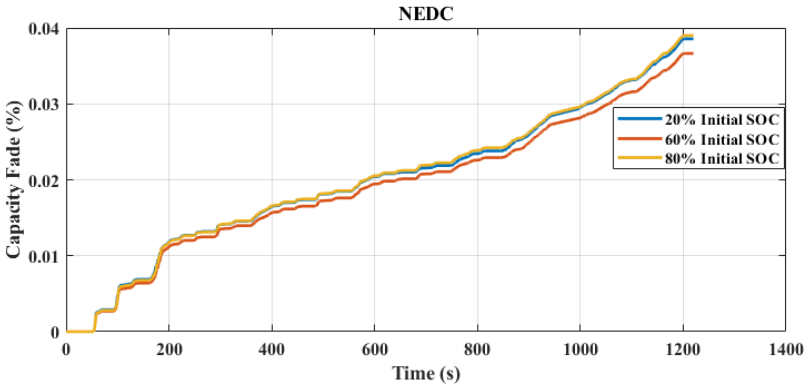

Fig. 14: NEDC Capacity Fade-Time graph

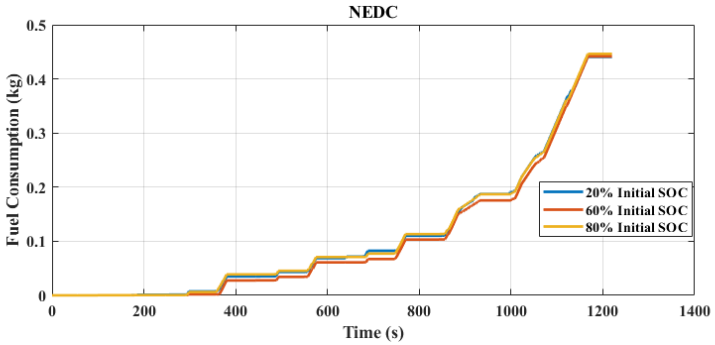

Fig. 15: NEDC Fuel Consumption-Time graph

Results for NEDC are given above in Figs. 13-15. NEDC is not as dynamic as WLTP and has lower average speed compared to HWFET. Required driving power is relatively low in NEDC compared to other two drive cycles. As a result of this, fuel consumption for different SOC levels is almost same according to Fig.15 and there is very small difference in battery degradation.

After ECMS is implemented and dataset is obtained. Two ANN controllers are designed to control ICE torque and speed. Capacity fade is used as one of the inputs for both controllers. Design of ANN controllers are explained in the next section.

4. Artificial Neural Network Based Controller Design

Matlab Neural Network Toolbox is used to design ANN controllers, torque request of the vehicle, SOC and capacity fade are the inputs of the controllers and the outputs are ICE torque and ICE speed. WLTP, HWFET and NEDC were run for three different initial SOC values. Number of data points for nine simulations is 11364. The dataset is divided as 70% for training, 15% for testing and 15% for validation. ANN settings are given below in Fig. 16.

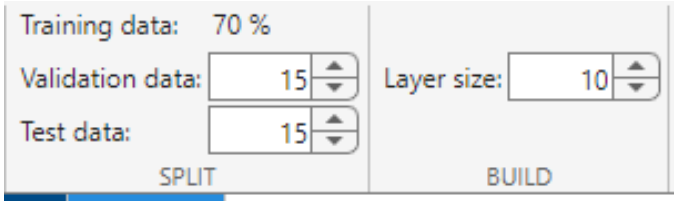

Fig. 16: ANN settings

Results of ANN controllers are given in the next section and compared with the results of ECMS for three drive cycles and three initial SOC scenarios.

5. Results and Discussion

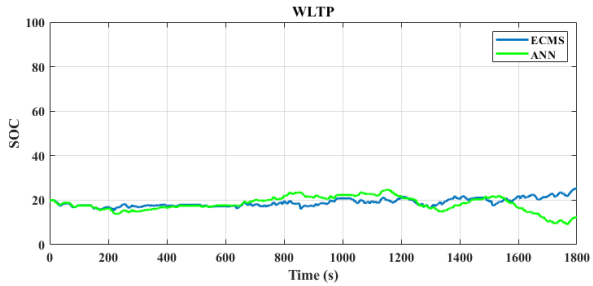

Fig. 17: SOC-Time graph for 20% Initial SOC in WLTP

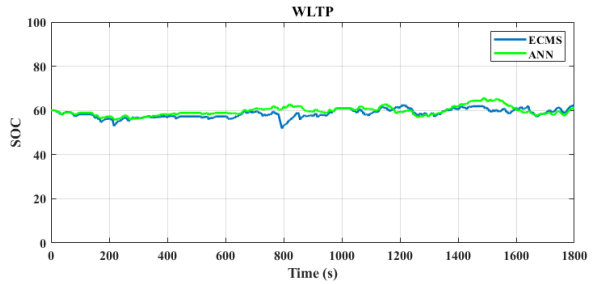

Fig. 18: SOC-Time graph for 60% Initial SOC in WLTP

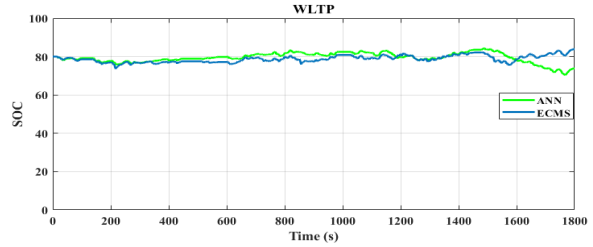

Fig. 19: SOC-Time graph for 80% Initial SOC in WLTP

Figs. 17-19 shows SOC profiles in WLTP for ECMS and ANN. As seen in these graphs, vehicle operates close to charge-sustaining mode when ANN controller is employed.

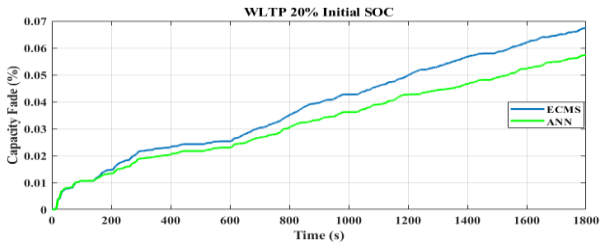

Fig. 20: Capacity Fade-Time graph for 20% Initial SOC in WLTP

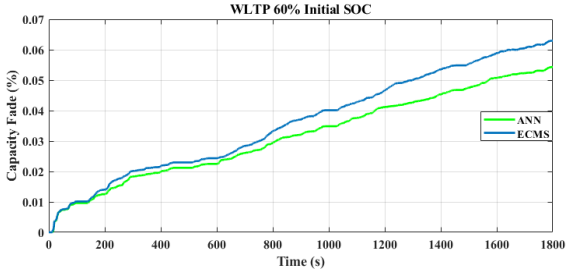

Fig. 21: Capacity Fade-Time graph for 60% Initial SOC in WLTP

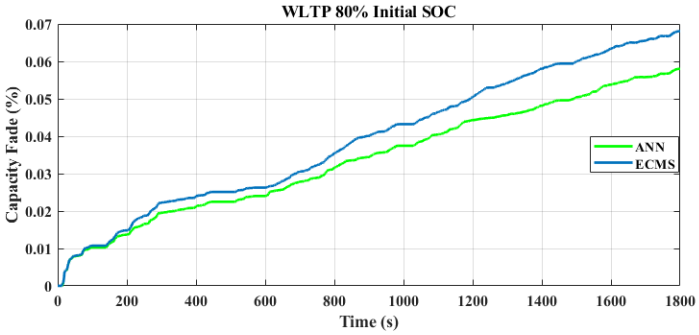

Fig. 22: Capacity Fade-Time graph for 80% Initial SOC in WLTP

Figs. 20-22 show capacity fade results of ANN and ECMS controllers for WLTP. Results show that capacity fade is reduced for all cases when ANN controller is employed.

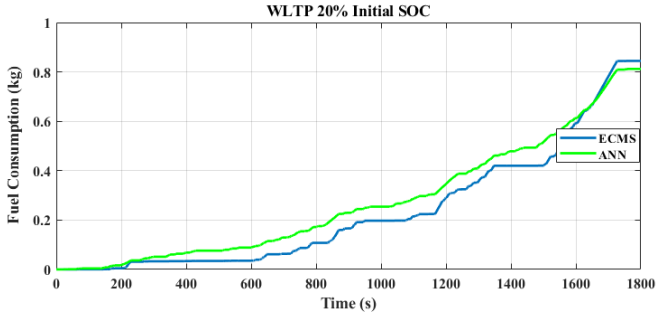

Fig. 23: Fuel consumption-Time graph for 20% Initial SOC in WLTP

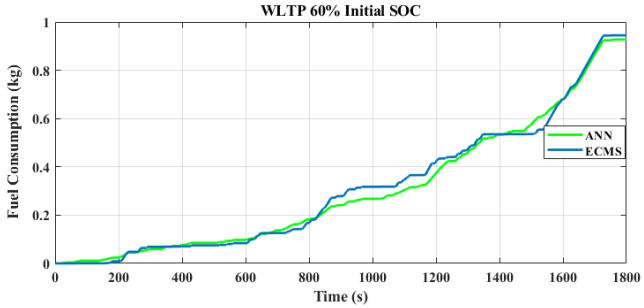

Fig. 24: Fuel consumption -Time graph for 60% Initial SOC in WLTP

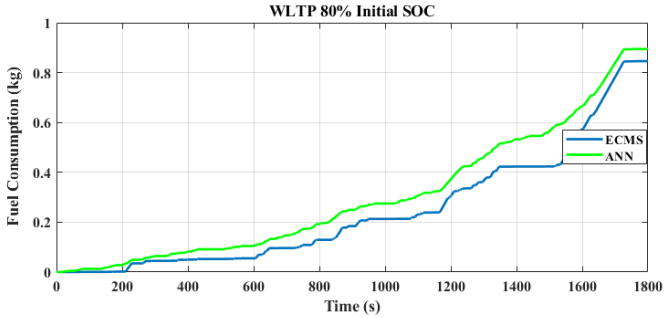

Fig. 25: Fuel consumption -Time graph for 80% Initial SOC in WLTP

Figs. 23-25 show fuel consumption results for WLTP. As seen in these results, fuel consumption is increased in just 80% initial SOC level. For other cases, fuel consumption is decreased slightly when ANN is used.

Results for HWFET are given below in Figs. 26-28 and Table 5. Figs. 26-28 show the SOC results and Table 5 shows capacity fade and fuel consumption at the end of drive cycle.

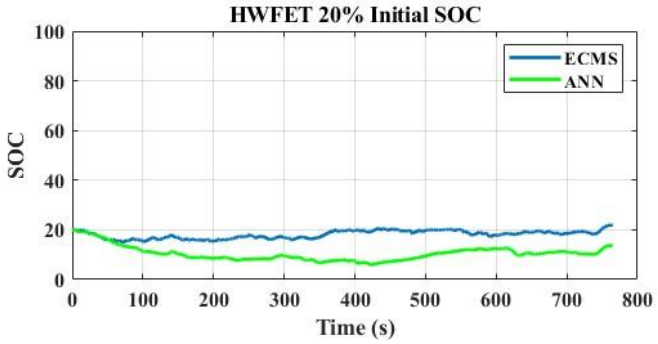

Fig. 26: SOC-Time graph for 20% Initial SOC in HWFET

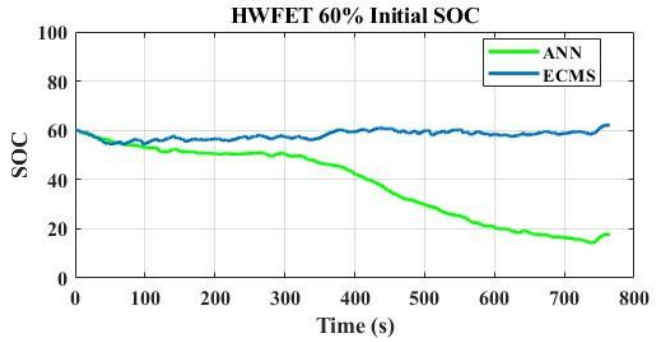

Fig. 27: SOC-Time graph for 60% Initial SOC in HWFET

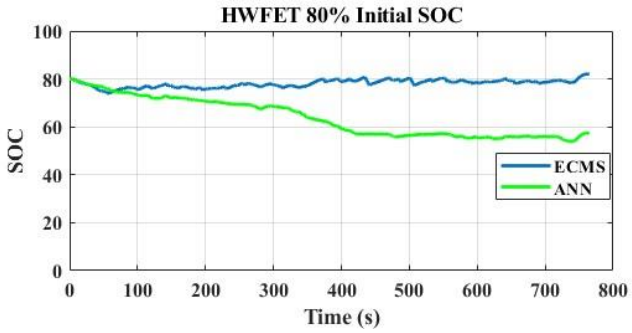

Fig. 28: SOC-Time graph for 80% Initial SOC in HWFET

Table 5: HWFET results

HWFET	ECMS	ANN
Capacity Fade for 20% Initial SOC (%)	0.0509	0.0310
Capacity Fade for 60% Initial SOC (%)	0.0457	0.0363
Capacity Fade for 80% Initial SOC (%)	0.0490	0.0299
Fuel Consumption for 20% Initial SOC (kg)	0.5837	0.6303
Fuel Consumption for 60% Initial SOC (kg)	0.6839	0.5294
Fuel Consumption for 80% Initial SOC (kg)	0.6862	0.5732

Results for HWFET show that capacity fade is decreased in all cases while fuel consumption is increased in one case. As seen in Figs. 26-28, the vehicle is operating in a charge depleting mode in HWFET, the only case that fuel consumption is increased is the initial SOC level of 20%. In this case, since the SOC level is low and vehicle is operating in a highway cycle, ICE must use more fuel to prevent total discharge of the battery, which results in an increase in fuel consumption. For intermediate and high SOC levels, the vehicle is depleting the battery, thus

reducing the fuel consumption. HWFET results show that for low SOC level, capacity fade is decreased as 39% and fuel consumption is increased as 7.9%. For medium SOC level, capacity fade is decreased as 20.5% and fuel consumption is decreased as 22.5 % and for high SOC level, capacity fade is decreased as 38.9% and fuel consumption is decreased as 16.46%.

Results for NEDC are given in Figs. 29-31 and Table 6.

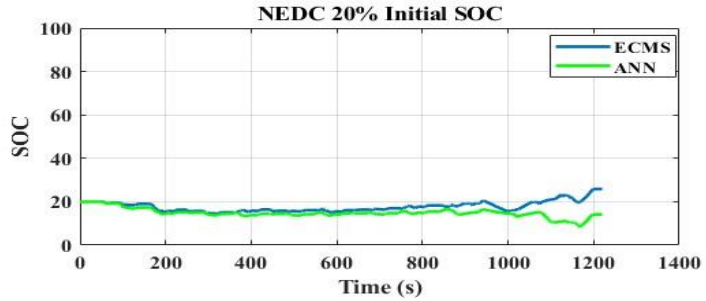

Fig. 29: SOC-Time graph for 20% Initial SOC in NEDC

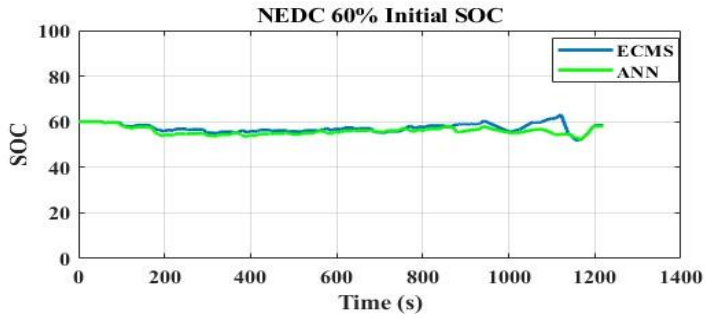

Fig. 30: SOC-Time graph for 60% Initial SOC in NEDC

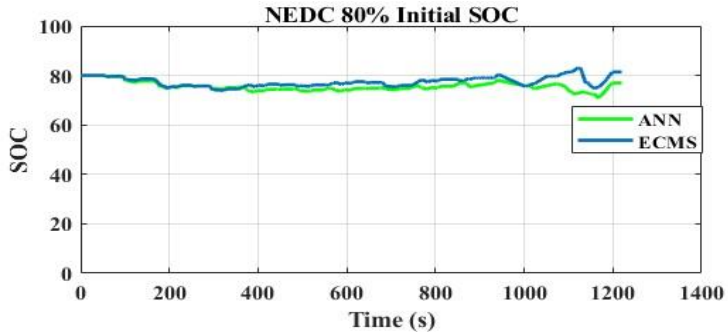

Fig. 31: SOC-Time graph for 80% Initial SOC in NEDC

Table 6: NEDC results

NEDC	ECMS	ANN
Capacity Fade for 20% Initial SOC (%)	0.0386	0.0332
Capacity Fade for 60% Initial SOC (%)	0.0366	0.0293
Capacity Fade for 80% Initial SOC (%)	0.0390	0.0336
Fuel Consumption for 20% Initial SOC (kg)	0.4406	0.3889
Fuel Consumption for 60% Initial SOC (kg)	0.4415	0.4052
Fuel Consumption for 80% Initial SOC (kg)	0.4462	0.3824

NEDC results show that capacity fade is decreased in all cases as well as fuel consumption. For low SOC level, capacity fade is decreased by 13.9% and fuel consumption is decreased by 11.73%. For medium SOC level, capacity fade is decreased by 19.94% and fuel consumption is decreased by 8.22%. For high SOC level, capacity fade is decreased by 13.84% and fuel consumption is decreased by 14.29%

6. Conclusion

Three different speed profiles are selected and applied for three different initial SOC values. In total, nine different cases are investigated and results of ECMS and ANN are compared in terms of SOC, capacity fade and fuel consumption. SOC profiles are included in the results because SOC is one of the parameters in the capacity fade model. This is why results are evaluated for charge-sustainability, degradation and fuel consumption. Results show that capacity fade of the battery is decreased in all cases when a control-oriented degradation model is used as an input for ANN controller. Fuel consumption is only increased in two cases. This shows that the proposed ANN-based controller can reduce battery degradation and fuel consumption depending on the initial SOC level and drive cycle.

For further research, the dataset size will be increased by using more drive cycles and capacity fade will be investigated further by aging the battery through simulations. Battery degradation is a very complex phenomenon and ANN has proven to be useful for battery health management. Training ANN for the further aging conditions and investigating battery degradation will be the focus of further research.

Acknowledgements

This research was supported by The Scientific and Technological Research Council of Turkey (TÜBİTAK) 2214-A - International Research Fellowship Programme for PhD Students.

References

[1] Gopal, A. R., Park, W. Y, Witt, M. and Phadke, A., “Hybrid- and battery-electric vehicles offer low-cost climate benefits in China,” Transportation Research Part D: Transport and Environment, vol. 62, pp. 362-371, July 2018.

[2] Buekers, J., Van Holderbeke, M., Bierkens, J., and Int Panis, L., “Health and environmental benefits related to electric vehicle introduction in EU countries,” Transportation Research Part D: Transport and Environment, vol. 33, pp. 26–38, December 2014.

[3] Kannangara, M., Bensebaa, F., and Vasudev, M.,” An adaptable life cycle greenhouse gas emissions assessment framework for electric, hybrid, fuel cell and conventional vehicles: Effect of electricity mix, mileage, battery capacity and battery chemistry in the context of Canada,” Journal of Cleaner Production, vol. 317, October 2021.

[4] Zou, Y., Lin, Z., Li, D., & Liu, Z. C., “Advancements in Artificial Neural Networks for health management of energy storage lithium-ion batteries: A comprehensive review,” Journal of Energy Storage, vol. 73, Part C, December 2023.

[5] Kang, L. W., Zhao, X., and Ma, J.,”A new neural network model for the state-of-charge estimation in the battery degradation process,” Applied Energy, vol. 121, pp. 20–27, May 2014.

[6] Chaoui, H., Ibe-Ekeocha, C. C., and Gualous, H.,” Aging prediction and state of charge estimation of a LiFePO4 battery using input time-delayed neural networks,” Electric Power Systems Research, vol. 146, pp. 189–197, May 2017.

[7] Lu, J., Xiong, R., Tian, J., Wang, C., Hsu, C. W., Tsou, N. T., Sun, F., and Li, J.,” Battery degradation prediction against uncertain future conditions with recurrent neural network enabled deep learning,” Energy Storage Materials, vol. 50, pp. 139–151. September 2022.

[8] Khamesipour, M., Chitsaz, I., Salehi, M., and Alizadenia, S., “Component sizing of a series hybrid electric vehicle through artificial neural network,” Energy Conversion and Management, vol. 254, February 2022.

[9] Xie, S., Hu, X., Qi, S., and Lang, K.,” An artificial neural network-enhanced energy management strategy for plug-in hybrid electric vehicles,” Energy, vol. 163, pp. 837–848, November 2018.

[10] Millo, F., Rolando, L., Tresca, L., and Pulvirenti, L.," Development of a neural network-based energy management system for a plug-in hybrid electric vehicle," Transportation Engineering, vol. 11, March 2023.
[11] Guzzella, L., and Amstutz, A. The QSS Toolbox Manual. 2005.
[12] Zhang, S., Hu, X., Xie, S., Song, Z., Hu, L., & Hou, C.," Adaptively coordinated optimization of battery aging and energy management in plug-in hybrid electric buses," Applied Energy, vol. 256, December 2019.
[13] G. Paganelli, Conception et commande d'une chaîne de traction pour véhicule hybride parallèle thermique et électrique. Ph.D. dissertation, Université de Valenciennes, Valenciennes (1999).
[14] Onori, S., Serrao, L. and Rizzoni, G. (2016) Hybrid Electric Vehicles Energy Management Strategies. Springer, London, pp. 65.